Inorg. Chem. **2009**, *48*, 3396−3407

Forum

Molecular Magnets Containing Wheel Motifs

Norihisa Hoshino,[†] Ayuk M. Ako,[‡] Annie K. Powell,*[,‡] and Hiroki Oshio*[,†]

Graduate School of Pure and Applied Sciences, University of Tsukuba, Tennodai 1-1-1, Tsukuba 305-8571, Japan, and Institut für Anorganische Chemie, Universität Karlsruhe, Engesserstrasse Geb. 30.45, D-76128 Karlsruhe, Germany

Received September 30, 2008

An overview of some compounds with structures that can be regarded as derived from an $\{Fe_7(\mu_3\text{-}OR)_6(\mu\text{-}OR)_6\}$ motif is presented. Many of these compounds act as single-molecule magnets. In addition, the results of a comprehensive study on the single-crystal structures, magnetism, and spin structures for five new iron compounds with structural components related to this are given. This serves to illustrate the methodology that can be used to unravel the complicated magnetic behavior of such systems. Thus, the alkoxo- and phenoxo-bridged multinuclear iron complexes, $[Fe^{II}_7(Hbmsae)_6(OMe)_6]Cl_2 \cdot 6H_2O$ (**6**), $[Fe^{II}Fe^{III}_6(bmsae)_6(\mu_3\text{-}OMe)_6]Cl_2 \cdot 23H_2O$ (**7**), $[NaFe^{III}_6(bmsae)_6(\mu_3\text{-}OMe)_6]Cl \cdot 30H_2O$ (**8**), $[Fe^{III}_3(bmsae)_3Cl_2(MeOH)(OMe)] \cdot MeOH \cdot Et_2O$ (**9**), and $[Fe^{III}_2(Hbmsae)_2(OMe)_2Cl_2][Fe_3(bmsae)_3(OMe)Cl_2(MeOH)]_2 \cdot 1.5MeOH$ (**10**), were prepared by the reactions of iron sources with Schiff base ligands (H_2bmsae = 5-bromo-3-methoxysalicylideneaminoethanol). Heptanuclear complexes of **6** and **7** have wheel structures in which six iron(II) and six iron(III) ions locate on the rim with the central iron(II) ions, respectively, while **8** also has a wheel structure with a diamagnetic sodium ion in the center. **9** is a trinuclear ferric complex with an incomplete cubic structure. In **10**, di- and trinuclear complexes exist in the crystal, where the trinuclear complex has an incomplete cubic structure similar to that of **9**. Magnetic susceptibility measurements revealed that **6** has an $S = 10$ spin ground state, while the antiferromagnetic interactions dominate in **7**−**10**.

Introduction

In the last few decades, the synthesis of polynuclear compounds containing magnetic transition-metal ions[1] has become the focus of intense research activities. The initial interest was as a result of their relevance to biological systems,[2] but more recently attention has turned to investigation of their potential as molecular species that can function as nanoscale magnetic particles or so-called single-molecule magnets (SMMs).[3] For example, iron and manganese clusters have been extensively studied as models for biological systems such as the iron-storage protein ferritin[4] and for the water-oxidizing complex in photosystem II,[5] respectively. Thus, the extensively studied $[Mn_{12}O_{12}(OAc)_{16}(H_2O)_4]$[3c] and $[Fe_8O_2(OH)_{12}(tacn)_6]Br$[3d] clusters represent prototypes of manganese and iron complexes showing SMM behavior. While clusters of other 3d metal ions can show SMM and other interesting magnetic behaviors,[6] it is fair to say that manganese clusters represent the largest source of systems with exotic magnetic properties. However, it is clear that

* To whom correspondence should be addressed. E-mail: oshio@chem.tsukuba.ac.jp (H.O.), powell@chemie.unikarlsruhe.de (A.K.P.).
† University of Tsukuba.
‡ Universität Karlsruhe.

(1) Müller, A.; Peters, F.; Pope, M. T.; Gatteschi, D. *Chem. Rev.* **1998**, 239, and references cited therein.
(2) (a) Lippard, S. J. *Angew. Chem., Int. Ed. Engl.* **1988**, *27*, 344. (b) Pope, M. T.; Müller, A. *Angew. Chem., Int. Ed. Engl.* **1991**, *30*, 34. (c) Katsoulis, D. E. *Chem. Rev.* **1998**, *98*, 359.
(3) (a) Gatteschi, D.; Sessoli, R. *Angew. Chem., Int. Ed.* **2003**, *42*, 268. (b) Christou, G.; Gatteschi, D.; Hendrickson, D. N. *MRS Bull.* **2000**, *25*, 66. (c) Sessoli, R.; Gatteschi, D.; Caneschi, A.; Novak, M. A. *Nature* **1993**, *365*, 141. (d) Barra, A.-L.; Debrunner, P.; Gatteschi, D.; Schulz, Ch. E.; Sessoli, R. *Europhys. Lett.* **1996**, *35*, 133.
(4) (a) Taft, K. L.; Delfs, C. D.; Papaefthymiou, G. C.; Foner, S.; Gatteschi, D.; Lippard, S. J. *J. Am. Chem. Soc.* **1994**, *116*, 823. (b) Crichton, R. R. *Angew. Chem., Int. Ed. Engl.* **1973**, *12*, 57. (c) Taft, K. L.; Papaefthymiou, G. C.; Lippard, S. J. *Science* **1993**, *259*, 1302.
(5) (a) Wieghardt, K. *Angew. Chem., Int. Ed. Engl.* **1994**, *33*, 725. (b) Debus, R. J. *Biochim. Biophys. Acta* **1992**, *1102*, 269. (c) Bruvig, G. W.; Thorp, H. H.; Crabtree, R. H. *Acc. Chem. Res.* **1991**, *24*, 311.

10.1021/ic801776w CCC: $40.75
Published on Web 04/13/2009

polynuclear iron compounds are an alternative source of interesting magnetic molecules, with several reported as SMMs in the literature.[7] In this article, we will discuss a class of these iron clusters where the compounds possess a common central heptanuclear core motif $\{Fe_7(\mu_3\text{-}OR)_6(\mu\text{-}OR)_6\}$, where R can be a proton or an organic residue on a deprotonated solvent such as water or methanol or else derives from an organic ligand, and the core derived from this when alternating metals on the periphery are removed, resulting in the tetranuclear "star" or "propeller" motif $\{Fe_4(\mu\text{-}OR)_6\}$. In addition to these hepta- and tetranuclear compounds, several higher-nuclearity compounds contain the central Fe_7 motif and can be thought of as higher generations toward the formation of the extended $Fe(OR)_n$ (n depends on the valence states of the iron) structure. Finally, the structures and properties of a set of new compounds derived from this Fe_7 motif are discussed.

Overview of Some Previous Studies

Fe_6 and Fe_7 Compounds. In previous studies, Saalfrank and co-workers have described an efficient, simple route for the template-mediated self-assembly of iron(III) ions and triethanolamine to give six- and eight-membered iron coronates $\{M[Fe_6(tea)_6]\}Cl$ (**1**; M = Li, Na) and $\{Cs[Fe_8(tea)_8]\}Cl$ (**2**).[8] Subsequently, a careful analysis of the construction plan of these systems was the basis for the rational design of six-membered iron coronands of the general formulation $[Fe_6\{R\text{-}CH_2N(CH_2CH_2O)_2\}_6X_6]$ (where R represents various side arms ranging from simple alkyl chains CH_3, $CH_3(CH_2)_{16}CH_2-$, to aromatic residues and X is a pseudohalide, Cl, NCS), obtained from a one-pot reaction of N-substituted diethanolamines with $FeCl_3$ and CaH_2 in tetrahydrofuran (THF).[9,10] As an example, the molecular structure of the ferric wheel $[Fe_6\{R\text{-}CH_2N(CH_2CH_2O)_2\}_6Cl_6]$ (**3**, where R = $CH_3(CH_2)_{16}CH_2-$) is given in Figure 1. The crystal structure of **3** contains one neutral discrete hexanuclear cluster with no solvate molecules.

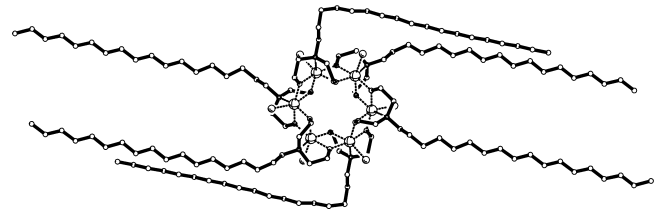

Figure 1. Structure of **3** in the crystal.

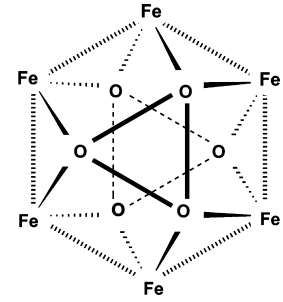

Figure 2. Schematic representation of the central Fe_6O_6 core of metallacoronands.

The six hexacoordinated iron centers of the centrosymmetric molecule are located in the corners of an almost regular hexagon (Figure 2), with the bridging ligands positioned alternately above and below the plane of the circle.

Although the structures of these iron(III) coronands are almost identical and have idealized S_6 or S_2 molecular symmetry, their variable side arms give rise to a whole variety of crystal packing motifs, creating various substructures.[9,10] For instance, the ferric wheel **3** has an idealized C_i molecular symmetry and crystallizes in the space group $P\bar{1}$, with all of the ferric wheels piled most simply in parallel, in cylindrical columns with mean intracolumnar midpont distances d of 12.6 Å, with all of the iron centers superimposed. Each column is surrounded by six parallel columns that are alternately dislocated by $^1/_3d$ and $^2/_3d$ against the central one. Additionally, an interesting packing pattern is observed with **3**, where the lipophilic tails of the ferric wheels interdigitate to create strands that by lateral van der Waals interactions pack to form 2D layers. The piling of these sheets creates the final 3D architecture of the crystal (Figure 3).

On the basis of the structural features presented by this compound, the morphology of monolayers formed upon adsorption of **3** endowed with extended linear hydrocarbon side chains on highly oriented pyrolytic graphite (HOPG) was investigated by in situ scanning tunneling microscopy (STM) at the liquid−solid interface. Figure 4 depicts the linear interdigitation of the alkyl chains of **3** to strands, where the molecules are attached to the monatomic graphite step horizontally. Only the molecule centers are visible as six bright spots that form a ring. Analyses of the STM images in Figure 4 (top) reveal that the ring diameter is ap-

(6) (a) Castro, S. L.; Sun, Z.; Grant, C. M.; Bollinger, J. C.; Hendrickson, D. N.; Christou, G. *J. Am. Chem. Soc.* **1998**, *120*, 2365. (b) Ochsenbein, S. T.; Murrie, M.; Rusanov, E.; Stoeckli-Evans, H.; Sekine, C.; Güdel, H. U. *Inorg. Chem.* **2002**, *41*, 5133, and references cited therein. (c) Yang, E.-C.; Wernsdorfer, W.; Hill, S.; Edwards, S. S.; Nakano, M.; Maccagnano, S.; Zakharov, L. N.; Rheingold, A. L.; Christou, G.; Hendrickson, D. N. *Polyhedron* **2003**, *22*, 1727. (d) Yang, E.-C.; Hendrickson, D. N.; Wernsdorfer, W.; Nakano, M.; Zakharov, L. N.; Sommer, R. D.; Rheingold, A. L.; Gairaud, M.-L.; Christou, G. *J. Appl. Phys.* **2002**, *91*, 7382. (e) Cadiou, C.; Murrie, M.; Paulsen, C.; Villar, V.; Wernsdorfer, W.; Winpenny, R. E. P. *Chem. Commun.* **2001**, 2666.

(7) (a) Oshio, H.; Hoshino, N.; Ito, T. *J. Am. Chem. Soc.* **2000**, *122*, 12602. (b) Boudalis, A. K.; Donnadieu, B.; Nastopoulos, V.; Modesto, C.-J. J.; Mari, A.; Sanakis, Y.; Tuchagues, J.-P.; Perlepes, S. P. *Angew. Chem., Int. Ed.* **2004**, *43*, 2266. (c) Benelli, C.; Parsons, S.; Solan, G. A.; Winpenny, R. E. P. *Angew. Chem., Int. Ed. Engl.* **1996**, *35*, 1825. (d) Jones, L. F.; Brechin, E. K.; Collison, D.; Helliwell, M.; Mallah, T.; Piligkos, S.; Rajaraman, G.; Wernsdorfer, W. *Inorg. Chem.* **2003**, *42*, 6601. (e) Powell, G. W.; Lancashire, H. N.; Brechin, E. K.; Collison, D.; Heath, S. L.; Mallah, T.; Wernsdorfer, W. *Angew Chem., Int. Ed.* **2004**, *43*, 5772. (f) Goodwin, J. C.; Sessoli, R.; Gatteschi, D.; Wernsdorfer, W.; Powell, A. K.; Heath, S. L. *J. Chem. Soc., Dalton Trans.* **2000**, 1835. (g) Powell, A. K.; Heath, S. L.; Gatteschi, D.; Pardi, L.; Sessoli, R.; Spina, G.; Del Giallo, F.; Pieralli, F. *J. Am. Chem. Soc.* **1995**, *117*, 2491. (h) Benelli, C.; Cano, J.; Journaux, Y.; Sessoli, R.; Solan, G. A.; Winpenny, R. E. P. *Inorg. Chem.* **2001**, *40*, 188.

(8) Saalfrank, R. W.; Bernt, I.; Uller, E.; Hampel, F. *Angew. Chem., Int. Ed. Engl.* **1997**, *36*, 2482.

(9) Saalfrank, R. W.; Deutscher, C.; Sperner, S.; Nakajima, T.; Ako, A. M.; Uller, E.; Hampel, F.; Heinemann, F. W. *Inorg. Chem.* **2004**, *43*, 4372.

(10) Ako, A. M.; Maid, H.; Sperner, S.; Zaidi, S. H. H.; Saalfrank, R. W.; Alam, M. S.; Müller, P.; Heinemann, F. W. *Supramol. Chem.* **2005**, *17*, 315.

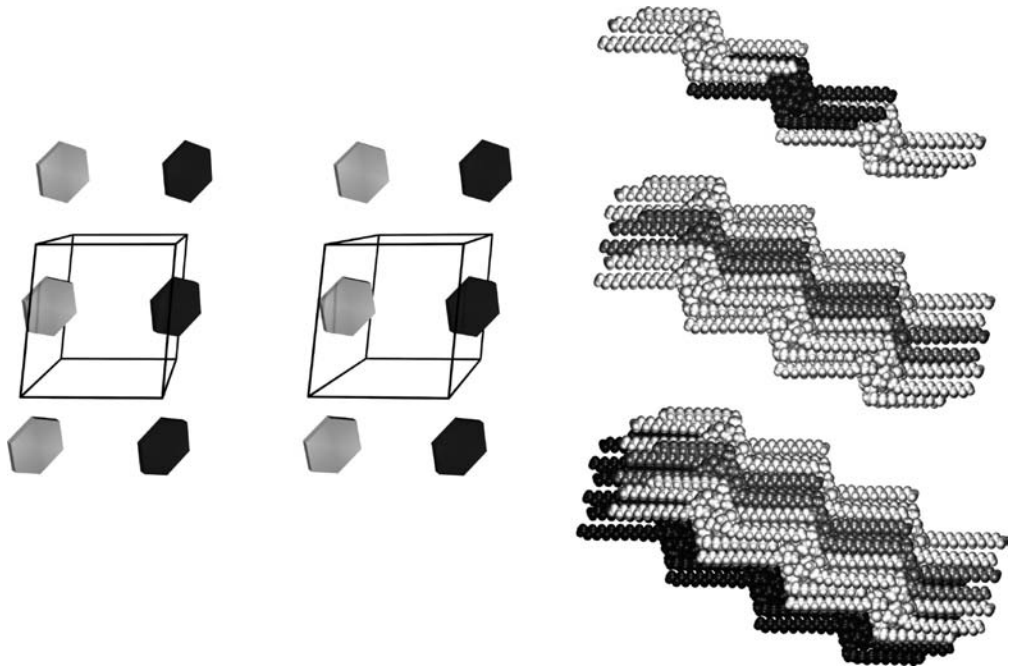

Figure 3. (Left) Schematic stereopresentation of the packing of the ferric wheels of **3**. (Right) Interdigitating alkyl chains, lateral interaction of 1D strands, piling of 2D layers, and the final 3D architecture. Midpoint distances (ferric wheels): 27.5 Å along chains, 13.0 Å between strands, 11.9 Å between planes.

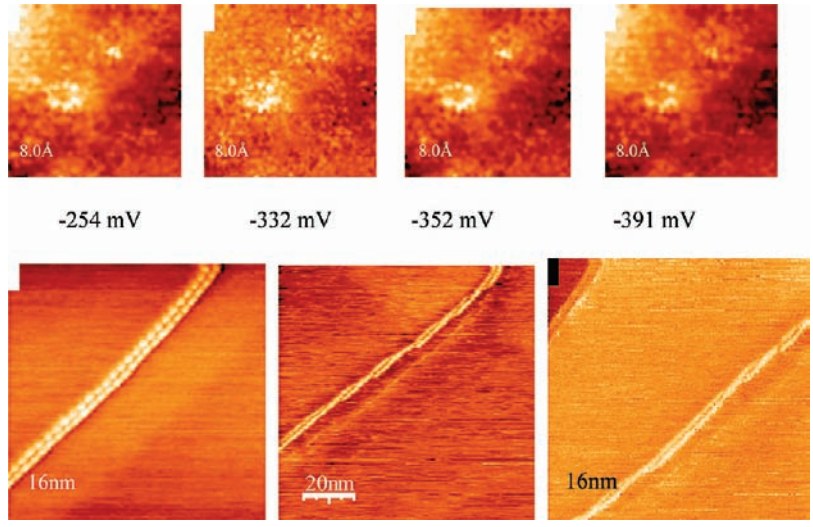

Figure 4. (Top) Display sections of a monolayer formed on the deposition of **3** on HOPG. (Bottom) Constant current STM topographies of **3** on HOPG showing the formation of double-linear superstructures (left) and double-helical superstructures (center and right). In both cases, there are a set-point voltage of 100 mV and a set-point current of 10 pA.

proximately 0.65 nm and the distance between neighboring peaks or spots is roughly 0.3 nm, conforming well to distances between iron ions of 0.632 nm across the ring and an average distance of 0.32 nm between neighboring iron ions, respectively, as obtained from the X-ray structure of **3**.

Recently, using Schiff base ligands with an alkyl alcohol group, Oshio and co-workers reported a high-spin (HS; $S = {}^{29}/_{2}$) heptanuclear mixed-valent iron(II,III) wheel, which showed SMM behavior.[11] In contrast to the large number of even-numbered iron(III) wheels known, which have been obtained from the reaction of suitable chelating ligands with preformed oxo-centered iron(III) triangles,[12] odd-numbered disklike all-iron(III) complexes are rare.[13] Such iron(III) complexes are interesting not only from a chemical and structural perspective but also because elucidation of their magnetic properties and spin topologies should help in understanding the magnetic properties of larger ferric systems. The arrangement in such a heptanuclear structure can be regarded as a ring comprising an even number of iron(III) ions with an additional central iron(III) ion, which can be predicted to allow for strong quantum-spin-frustration effects due to competing nearest-neighbor exchange interac-

(11) Oshio, H.; Hoshino, N.; Ito, T.; Nakano, M.; Renz, F.; Gütlich, P. *Angew. Chem., Int. Ed.* **2003**, *42*, 223, and references cited therein.

(12) (a) Cañada-Vilalta, C.; O'Brien, T. A.; Brechin, E. K.; Pink, M.; Davidson, E. R.; Christou, G. *Inorg. Chem.* **2004**, *43*, 5505. (b) Murugesu, M.; Abboud, K. A.; Christou, G. *Dalton Trans.* **2003**, 4552. (c) Jones, L. F.; Jensen, P.; Moubaraki, B.; Cashion, J.; Berry, K. J.; Murray, K. S. *Dalton Trans.* **2005**, 3344.

Scheme 1. Triethanolamine, ($teaH_3$) H_3L^1 (Left), *n*-Butyldiethanolamine, ($bdeaH_2$) H_2L^2 (Center), and Phenyldiethanolamine, ($PhdeaH_2$) H_2L^3 (Right)

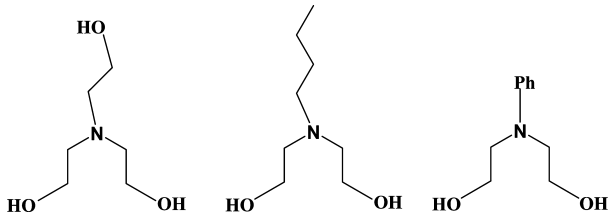

tion paths. In fact, the exchange-coupling situation realized in such clusters bears a close analogy to the so-called frustrated Heisenberg star introduced by Richter and Voigt as a rare example of an exactly solvable quantum-spin model with frustration.[14]

We recently described three isostructural disklike heptanuclear iron(III) compounds of the general formula $[Fe^{III}_7(\mu_3\text{-}O)_3(L)_3(\mu\text{-}O_2CCMe_3)_6(\eta^1\text{-}O_2CCMe_3)_3(H_2O)_3]$, where L represents a di- or triethanolamine moiety (Scheme 1), which can be regarded in terms of a three-blade-propeller topology, with the central iron atom representing the axle or axis of the propeller.[15] Exemplarily, the structure and core of the *N*-*n*-butyldiethanolamine derivative (**4**) are given in Figure 5.

This motif corresponds to the theoretical model of a frustrated Heisenberg star, which is one of the very few solvable models in the area of frustrated quantum-spin systems and is related to the motif found in the Fe_4 systems. It should be stressed that in these cases in the Fe_7 motif the iron centers are no longer coplanar. The magnetic behavior was studied using bulk susceptibility measurements, and subsequent electron paramagnetic resonsance results led to the assignment of an $S = {}^5/_2$ ground spin state with a D value of -0.43 cm^{-1}.[16] We are currently investigating this motif further using Mössbauer spectroscopy.

Fe_4 Compounds. Relatively simple molecules based on a star-shaped or propeller motif, where a central metal is octahedrally linked to three further ones via oxygen bridges, have been shown to display both high ground-state spins and sometimes SMM behavior. These compounds also offer the possibility of identifying the geometric requirements that favor various types of magnetic behavior. In this respect, the use of HS d^5 transition-metal ions such as iron(III) and manganese(II) can theoretically lead to large spin values even for quite small numbers of paramagnetic centers. A simple Fe^{III}_4 motif has been shown to produce a relatively large spin by

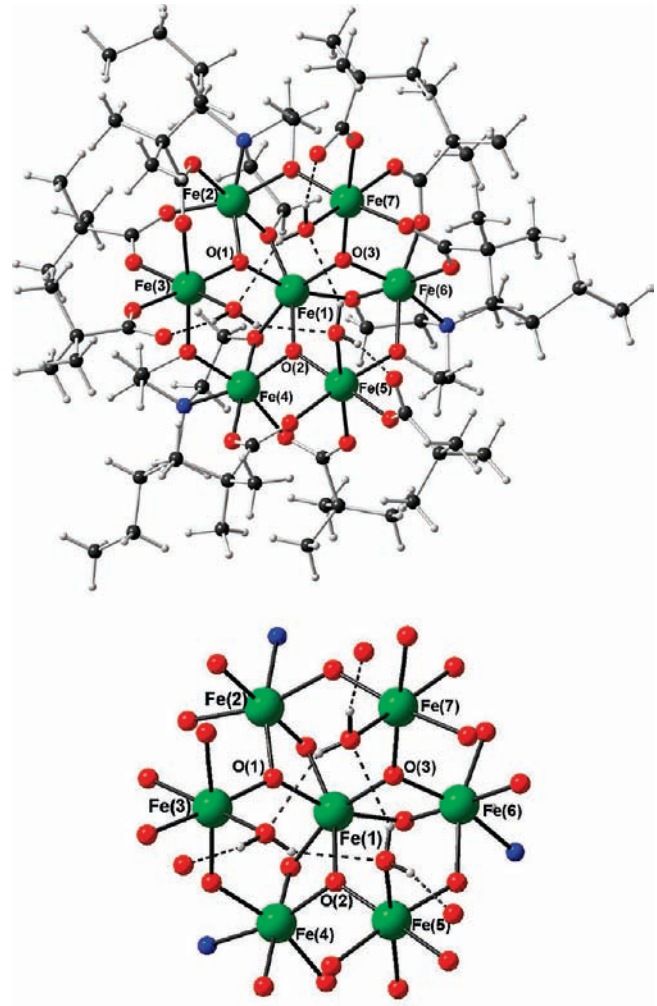

Figure 5. (Top) Molecular structure of **4** in the crystal. (Bottom) Core of **4**. Color code: green, Fe; red, O; blue, N; black, C; white, H.

Gatteschi et al.[17] in $[Fe_4(OCH_3)_6(dpm)_6]$ (where Hdpm = dipivaloylmethane), by Saalfrank et al.[18] in $[Fe_4(mde)_6]$ (where H_2mde = *N*-methyldiethanolamine), and by Mallah et al.[19] in $[Fe_4(thme)_2(C_3H_7OH)_6Cl_6]$ where H_3thme = tris(hydroxymethyl)ethane. These molecules have $S = 5$ ground spin states, which can be rationalized by having the central metal ion in an antiparallel spin orientation to the three others, as shown in Figure 6.

Such molecules are also found to exhibit SMM behavior, and the magnetic behavior of the molecule, $[Fe_4(OCH_3)_6(dpm)_6]$, was subsequently enhanced by replacing the six

(13) Jones, L. F.; Jensen, P.; Moubaraki, B.; Berry, K. J.; Boas, J. F.; Pilbrow, J. R.; Murray, K. S. *J. Mater. Chem.* **2006**, *16*, 2690.
(14) (a) Richter, J.; Voigt, A. *J. Phys. A: Math. Gen.* **1994**, *27*, 1139. (b) Richter, J.; Voigt, A.; Krüger, S. E.; Gross, C. *J. Phys. A: Math. Gen.* **1996**, *29*, 825.
(15) Ako, A. M.; Waldmann, O.; Mereacre, V.; Hewit, I. J.; Klöwer, F.; Anson, C. E.; Güdel, H. U.; Powell, A. K. *Inorg. Chem.* **2007**, *46*, 756.
(16) Ako, A. M.; Burger, B.; Waldmann, O.; Mereacre, V.; Anson, C. E.; Powell, A. K. unpublished results.
(17) (a) Barra, A.-L.; Caneschi, A.; Cornia, A.; Fabrizi de Biani, F.; Gatteschi, D.; Sangregorio, C.; Sessoli, R.; Sorace, L. *J. Am. Chem. Soc.* **1999**, *121*, 5302. (b) Sessoli, R.; Caneschi, A.; Gatteschi, D.; Sorace, L.; Cornia, A.; Wernsdorfer, W. *J. Magn. Magn. Mater.* **2001**, *226*−*230*, 1954.
(18) (a) Saalfrank, R. W.; Bernt, I.; Chowdhry, M. M.; Hampel, F.; Vaughan, G. B. M. *Chem.*−*Eur. J.* **2001**, *7*, 2765. (b) Saalfrank, R. W.; Scheurer, A.; Bernt, I.; Heinemann, F. W.; Postnikov, A.; Schünemann, V.; Trautwein, A. X.; Alam, M. S.; Rupp, H.; Müller, P. *Dalton Trans.* **2006**, 2865.
(19) Moragues-Cánovas, M.; Rivière, É.; Ricard, L.; Paulsen, C.; Wernsdorfer, W.; Rajaraman, G.; Brechin, E. K.; Mallah, T. *Adv. Mater.* **2004**, *16*, 1101.
(20) Cornia, A.; Fabretti, A. C.; Garrisi, P.; Mortalò, C.; Bonacchi, D.; Gatteschi, D.; Sessoli, R.; Sorace, L.; Wernsdorfer, W.; Barra, A. *Angew. Chem., Int. Ed.* **2004**, *43*, 1136.

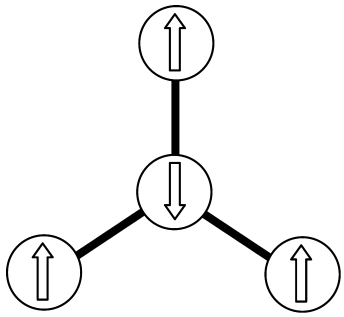

Figure 6. Spin structure leading to the $S = 5$ ground state of Fe_4 propellers.

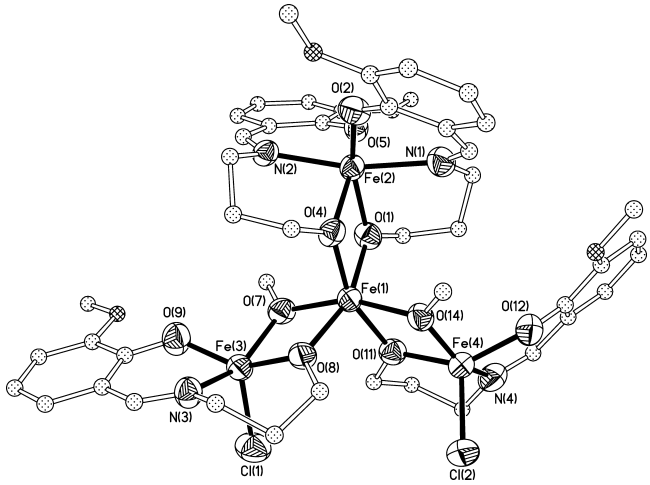

Figure 7. Structure of **5**.

Scheme 2. Schiff Base Ligand, L, Formed by Condensing *o*-Vanillin with 3-Amino-1-propanol

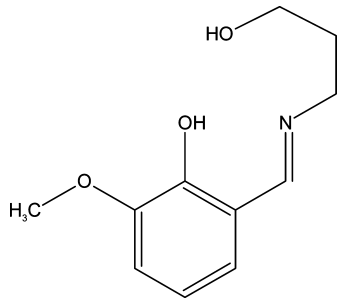

bridging methoxy groups with two thme^{3-} ligands to give $Fe_4(thme)_2(dpm)_6$.[20] We investigated a compound with a similar core motif but using a different ligand system (Scheme 2).

We found that the compound $[Fe_4(vap)_4(\mu\text{-}OMe)_2Cl_2]$ (**5**)[21] (Figure 7), which contains a similar Fe_4O_6 core with an $S = 5$ ground spin state and for which the metric parameters, spin state, and anisotropy would suggest that SMM behavior should be observed (see Table 1), turned out not to show any of the characteristics expected. Even micro-SQUID measurements (Figure 8) showed no evidence of hysteresis down to 0.04 K, posing the question, "what makes a SMM?"

A careful examination of the detailed bonding situation does not provide any obvious answer. Although for

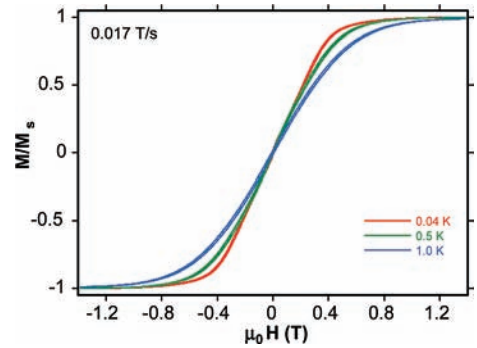

Figure 8. Micro-SQUID measurements on **5** down to 0.04 K.

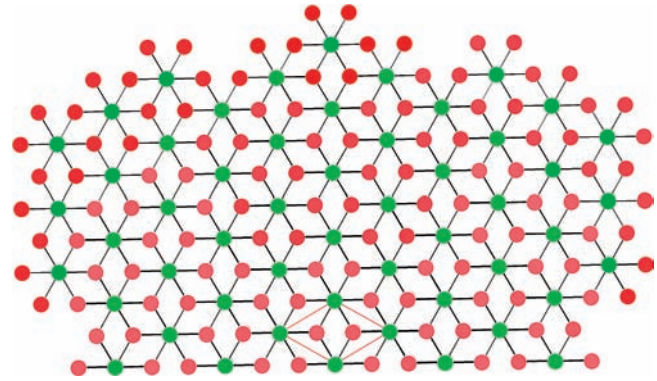

Figure 9. AB_2 lattice as seen in the brucite, $Mg(OH)_2$, structure. The metal atoms are the green spheres, and the oxygen atoms are the red spheres.

$[Fe_4(thme)_2(dpm)_6]$ it was suggested that the bite angles for the central iron are responsible for the enhanced SMM behavior,[20] here the corresponding angles should be even more favorable. Whereas in the case of $[Fe_4(thme)_2(dpm)_6]$ D_{3d} symmetry is crystallographically imposed, for the SMMs $[Fe_4(CH_3O)_6(dpm)_6]$ and $[Fe_4(thme)_2(C_3H_7OH)_6Cl_6]$,[19] as for compound **5**, this is not the case. The effect of trigonal compression and rotation on the magnetic anisotropy of an FeO_6 chromophore such as that found at the center of these complexes and its effect on SMM behavior has been discussed previously.[20−23] The two types of distortion are defined by the angles θ and φ, whose values are 57.74° and 60°, respectively, for a regular octahedron. Angular overlap model calculations show that trigonal compression, quantified by the angle θ, leads to a positive single ion D value and rotation of an octahedral face about the three-fold axis, quantified by φ, favors a negative D value.[23] Comparing the parameters for all four compounds again leads to the conclusion that there is no reason why compound **5** should not show SMM behavior. For example, compound **5** has a larger extent of trigonal rotation ($\varphi = 36.1°$) than $[Fe_4(CH_3O)_6(dpm)_6]$ ($\varphi = 41.8°$) for essentially the same extent of trigonal compression ($\theta = 57.4°$ and 57.3°, respectively). In fact, the only significant difference in the structure of **5** is the presence of the two five-coordinate peripheral iron atoms. Does this fact somehow abolish the SMM behavior? One possibility is that for compound **5** there is a large transverse anisotropy (E term) that is allowed

(21) Madhu, N. T.; Jin-Kui, T.; Hewitt, I. J.; Clérac, R.; Wernsdorfer, W.; van Slageren, J.; Anson, C. E.; Powell, A. K. *Polyhedron* **2005**, *24*, 2864.

(22) Muetterties, E. L.; Guggenberger, L. J. *J. Am. Chem. Soc.* **1974**, *96*, 1748.

(23) Gatteschi, D.; Sorace, L. *J. Solid State Chem.* **2001**, *159*, 253.

Table 1. Selected Bond Angles and Bond Lengths and Estimated Magnetic Parameters

	$[Fe_4(vap)_4(CH_3O)_2Cl_2]$ (**2**)	$[Fe_4(CH_3O)_6(dpm)_6]$	$[Fe_4(thme)_2(dpm)_6]$	$[Fe_4(thme)_2(C_3H_7OH)_6Cl_6]$
ref	21	3	7	6
Fe−O−Fe/deg	104.59−107.13	104.2−104.4	102.9	105.0−105.2
Fe···Fe/Å	3.147−3.204	3.146−3.133	3.086	3.157−3.158
θ/deg	57.4	57.3	54.1	54.4
φ/deg	36.1	41.8	29.2	25.5
g	2.00	1.97	2.00	1.98
J/k_B/K	−21.0	−15.2	−11.9	−20.6
D/k_B/K	−0.45	−0.3	−0.6	−0.46

by symmetry in this case. A similar situation where a Ni_4 cluster with a negative D term fails to show SMM behavior has been observed and found to be the result of a large E term.[24]

Larger Compounds Containing Fe_7 Cores. We found that a useful route to larger compounds with the Fe_7 core motif was to find ways of limiting the natural hydrolysis reaction of iron(III) ions in water by supplying chelating ligands. We can imagine this process as beginning at the atomic level with iron(III) ions in the form of the hexaaqua ion $[Fe(H_2O)_6]^{3+}$. Under normal conditions, a variety of hydrolysis reactions would lead to the precipitation of an amorphous hydroxide, which would then age into well-defined mineral phases such as the oxyhydroxide goethite and finally transform into the thermodynamically most stable oxide, hemeatite.[25]

We have observed that supplying tripodal chelating ligands of the general form $N(RCOOH)_2R'$ (where R′ can be any organic residue) to such solutions can halt this process by stabilizing captured intermediate phases consisting of close-packed cores that are portions of the brucite structure, exemplified by $Mg(OH)_2$, encased in a shell of the ligand units.[26,27] It is worth looking at this hydrolysis process in more detail.

The brucite structure is an AB_2 lattice made up of close-packed hydroxide (B) layers that are arranged as double strips, and the metal(II) ions (A) sit in octahedral holes between these strips so that each hydroxide bridges three metal ions, as shown in Figure 9. In the hydrolysis process, we can imagine the starting point (first generation) to be a hexaaqua metal ion that, upon production of the hexahydroxo metal ion, will link to a further six metal ions (second generation), and the process will continue through hydroxide production and coordination to a further 6 metal centers (third generation), then 12 (fourth generation), and so on, as can be recognized in Figure 9. Aggregates containing portions of such core structures have been structurally characterized for a variety of metal ions.[26−39] Clearly, for the metal(III) examples, an infinite brucite structure is not possible on the grounds of charge imbalance and the shell of ligands coordinated to the outermost metal ions of the hydroxide lattice in the observed aggregates can help to balance this. A further pertinent point is that removal of half the protons from the double strips of hydroxides in brucite leads to a layer of the α-oxyhydroxide structure, exemplified for iron(III) by goethite, α-FeO(OH), itself the precursor to the thermodynamically most stable phase, hemeatite. We can thus think of such aggregates as metastable intermediates that are trapped through the process of crystallization. For iron(III), these aggregates prove to be magnetically interesting because, although the overall coupling is antiferromagnetic, the pairwise interactions are unequal in magnitude over the whole molecule, leading to residual ground-state spins of up to $^{33}/_2$ and displaying hysteresis of the magnetization.[27,40−42]

The first examples synthesized were cluster compounds Fe_{17} and Fe_{19}, which were found to cocrystallize in a 1:1 ratio and display an unusual magnetic behavior as a result of both compounds possessing HS ground states. The ligand used was $H_3heidi = N(CH_2CH_2OH)(CH_2COOH)_2$. In these molecules, the first two generations in the formation of the brucite lattice lead to the central Fe_7 core, which is encapsulated by a ring of 10 or 12 Fe/ligand units where the iron(III) centers are held together in pairs through the dinucleating alcohol arm of the ligand. The analysis of the magnetic behavior of the system was complicated by the presence of the two related but different clusters, but we were able to conclude that one cluster should have a ground state

(24) Sieber, A.; Boskovic, C.; Bircher, R.; Waldmann, O.; Ochsenbein, S. T.; Güdel, H. U.; Kirchner, N.; van Slageren, J.; Wernsdorfer, W.; Neels, A.; Stoeckli-Evans, H.; Janssen, S.; Juranyi, F.; Mutka, H. *Inorg. Chem.* **2005**, *44*, 4315.

(25) Cornell, R. M.; Schwertmann, U. *The Iron Oxides*; VCH: Weinheim, Germany, 1996.

(26) Heath, S. L.; Powell, A. K. *Angew. Chem., Int. Ed. Engl.* **1992**, *31*, 191.

(27) Goodwin, J. C.; Sessoli, R.; Gatteschi, D.; Wernsdorfer, W.; Powell, A. K.; Heath, S. L. *J. Chem. Soc., Dalton Trans.* **2000**, 1835.

(28) Bolcar, M. A.; Aubin, S. M. J.; Folting, K.; Hendrickson, D. N.; Christou, G. *Chem. Commun.* **1997**, 1485.

(29) Tesmer, M.; Müller, B.; Vahrenkamp, H. *Chem. Commun.* **1997**, 721.

(30) Abbati, G. L.; Cornia, A.; Fabretti, A. C.; Caneschi, A.; Gatteschi, D. *Inorg. Chem.* **1998**, *37*, 3759.

(31) Oshio, H.; Hoshino, N.; Ito, T.; Nakano, M.; Renz, F.; Gütlich, P. *Angew. Chem., Int. Ed.* **2003**, *42*, 223.

(32) Boulmaaz, S.; Papiernik, R.; Hubertpfalzgraf, L. G.; Vaissermann, J.; Daran, J. C. *Polyhedron* **1992**, *11*, 1331.

(33) Pohl, I. A. M.; Westin, L. G.; Kritikos, M. *Chem.—Eur. J.* **2001**, *7*, 3438.

(34) Brockman, J. T.; Huffman, J. C.; Christou, G. *Angew. Chem., Int. Ed.* **2002**, *41*, 2506.

(35) Murrie, M.; Stoeckli-Evans, H.; Güdel, H. U. *Angew. Chem., Int. Ed.* **2001**, *40*, 1957.

(36) Brechin, E. K.; Harris, S. G.; Harrison, A.; Parsons, S.; Whittaker, A. G.; Winpenny, R. E. P. *Chem. Commun.* **1997**, 653.

(37) Goodwin, J. C.; Teat, S. J.; Heath, S. L. *Angew. Chem., Int. Ed.* **2004**, *43*, 4037.

(38) Heath, S. L.; Jordan, P. A.; Johnson, I. D.; Moore, G. R.; Powell, A. K.; Helliwell, M. *J. Inorg. Biochem.* **1995**, *59*, 785.

(39) Schmitt, W.; Baissa, E.; Mandel, A.; Anson, C. E.; Powell, A. K. *Angew. Chem., Int. Ed.* **2001**, *40*, 3578.

(40) Powell, A. K.; Heath, S. L.; Gatteschi, D.; Pardi, L.; Sessoli, R.; Spina, G.; Del Giallo, F.; Pieralli, F. *J. Am. Chem. Soc.* **1995**, *117*, 2491.

(41) Price, D. J.; Lionti, F.; Ballou, R.; Wood, P. T.; Powell, A. K. *Philos. Trans. R. Soc. London, Ser. A* **1999**, *357*, 3099.

(42) Affronte, M.; Sessoli, R.; Gatteschi, D.; Wernsdorfer, W.; Lasjaunias, J. C.; Heath, S. L.; Powell, A. K.; Fort, A.; Rettori, A. *J. Phys. Chem. Solids* **2004**, *65*, 745.

corresponding to $S = {}^{33}/_{2}$, which at the time was the highest spin observed on a molecule. The analysis also suggested that the other cluster should have an $S = {}^{25}/_{2}$ ground state. Subsequently, we found that by slight modifications to the encapsulating ligands, which was simply to add R groups to the alcohol arm of the molecule, it was possible to crystallize compounds only containing Fe_{19} clusters. The analysis of the magnetic behavior for these confirmed that the Fe_{19} components carry the highest spins and also behave as SMMs. Furthermore, adapted density functional theory calculations on the original system could rationalize the magnetic behavior in terms of the Fe_{17} clusters having an $S = {}^{25}/_{2}$ ground state and the Fe_{19} clusters an $S = {}^{35}/_{2}$ ground state. A relatively simple spin model, where the central Fe^{III}_{7} core has all iron(III) ions antiferromagnetically coupled, can be used to arrive at the suggested spin ground states. Furthermore, the presence of anisotropy in the system and the probability that there are small intercluster interactions can account for the experimental result of $S = {}^{33}/_{2}$ being slightly lower than the predicted value, although it is not necessarily expected that a simple spin model must work.

We were subsequently able to apply such a spin model to help in describing the magnetic behavior of another compound, Fe_{13}. Here the tripodal proligand nitrilotripropionic acid, $H_3ntp = N(CH_2CH_2COOH)_3$, was used and traps the Fe_{13} aggregates (Figure 10). Here the central core of $\{Fe_7(OH)_6\}^{15+}$ again corresponds to the first two generations of the brucite lattice, but then the final six iron(III) centers of the third generation are connected to this via six triply bridging oxide rather than hydroxide ions. These oxides provide an important structural element because they link three metal ions in a trigonal rather than a pyramidal fashion. This has the result that the final six iron centers are disposed above and below the core, alternating with the hydroxides and giving a "diabolo" arrangement, and means that they form a trigonal-antiprismatic arrangement, which becomes important in the hierarchical structure seen in the compound. In the 3D structure, there are two almost identical aggregates with formulas $[Fe_{13}(\mu_3\text{-}OH)_6(\mu_3\text{-}O)_6(Hntp)_8(H_2O)_6]^{5+}$, cluster A, and $[Fe_{13}(\mu_3\text{-}OH)_6(\mu_3\text{-}O)_6(Hntp)_8]^{5+}$, cluster B, in a 1:2 ratio. The difference between these lies in the way clusters A and B are linked together through peripheral carboxylate bridges, which can be single or double. The resulting structure has ABBABBA layers and can be described as very close-packed because the A clusters sit in octahedral holes between two layers of B clusters and the B clusters sit in octahedral holes between a layer of A clusters and a layer of B clusters (Figure 10). The octahedral arrangements result from the trigonal-antiprismatic arrangement of the peripheral iron centers on each Fe_{13} unit.

The magnetic behavior of this system turns out to be extremely challenging to interpret, probably as a result of the hierarchical nature of the structure, with the connections between clusters allowing for transfer of magnetic information. From the analysis of the Fe_{17} and Fe_{19} systems, we expect that the clusters are antiferromagnetically coupled, with the strongest interactions through the μ_3-O bridges giving a ground spin state of $S = {}^{5}/_{2}$. The low-temperature magnetic behavior suggests that there are two regimes in operation. At lower fields, the molecular components dominate with $S = {}^{5}/_{2}$ SMM behavior. At higher fields, the intercluster interactions become important and the system becomes very difficult to describe. This compound represents the realization of the production of an ordered array of nanomagnets using chemical processes rather than physical fabrication techniques.

Syntheses and Characterization of New Examples of Multinuclear Iron Complexes with Schiff Bases

A simple Schiff base with bridging groups is a powerful tool for the construction of multinuclear complexes, and such Schiff bases can also be applicable to the assembly of heterometal ions into multinuclear systems. In this section, a series of multinuclear iron complexes with Schiff bases is presented.

Syntheses. A ligand H_2bmsae (=5-bromo-3-methoxysalicylideneaminoethanol) was prepared by the condensation reaction of 5-bromo-3-methoxysalicylaldehyde with aminoethyl alcohol. All reactions were carried out in a methanol solution and under an aerobic atmosphere except for **6**, and the reaction scheme is shown in Scheme 3. Complexes **6**−**10** were synthesized by the reactions of iron chloride with H_2bmsae in the presence of triethylamine or sodium methoxide. The reaction of H_2bmsae, triethylamine, with iron(II) chloride in a 1:2:1 molar ratio gave a dark-brown solution. From this solution, dark-brown hexagonal plates of **6** were obtained under a nitrogen atomsphere, while under an aerobic atmosphere, mixed valence **7** was obtained as black blocks. The reaction of H_2bmsae with triethylamine, sodium methoxide, and iron(II) chloride in a $1{:}4{:}{}^{1}/_{6}{:}1$ molar ratio yielded black blocks of **8**. The reaction of H_2bmsae, triethylamine, and iron(II) chloride in a 1:2:1 molar ratio results in a dark-brown solution, giving black cubes of **9** by Et_2O diffusion, and the concentration of the solution affords black rods of **10**.

Descriptions of Structures. Core structures of **6**−**10** are shown in Figure 11, and the crystal data are summarized in Table 2. The oxidation states of the iron ions were assigned by charge considerations, coordination bond lengths, and Mössbauer data.

$[Fe^{II}_{7}(Hbmsae)_6(OMe)_6]Cl_2\cdot 6H_2O$ (**6**) crystallized in the trigonal space group of $R\bar{3}$. A complex molecule of **6** locates on the $\bar{3}$ axis and has a wheel structure composed of seven iron ions on the same plane. The heptanuclear core has six μ_2-phenoxo-bridged iron(II) ions on the rim, which are linked to the cetral iron(II) ion by six μ_3-methoxy bridges. Each iron(II) ion on the rim adopts an N_1O_5 configuration from the Schiff base and methoxide. Note that the protonated alcohol in $Hbmsae^-$ remains uncoordinated. Coordination bond lengths about the iron(II) (Fe_2) ions on the rim are in the range of 2.040(3)−2.336(4) Å, while the octahedral central iron ion (Fe_1) has the coordination bond length of 2.150(3) Å.

$[Fe^{II}Fe^{III}_{6}(bmsae)_6(\mu_3\text{-}OMe)_6]Cl_2\cdot 23H_2O$ (**7**) and $[NaFe^{III}_{6}(bmsae)_6(\mu_3\text{-}OMe)_6]Cl\cdot 30H_2O$ (**8**) are isomorphous with the cubic space groups of $Ia\bar{3}d$, and their cores have cyclic

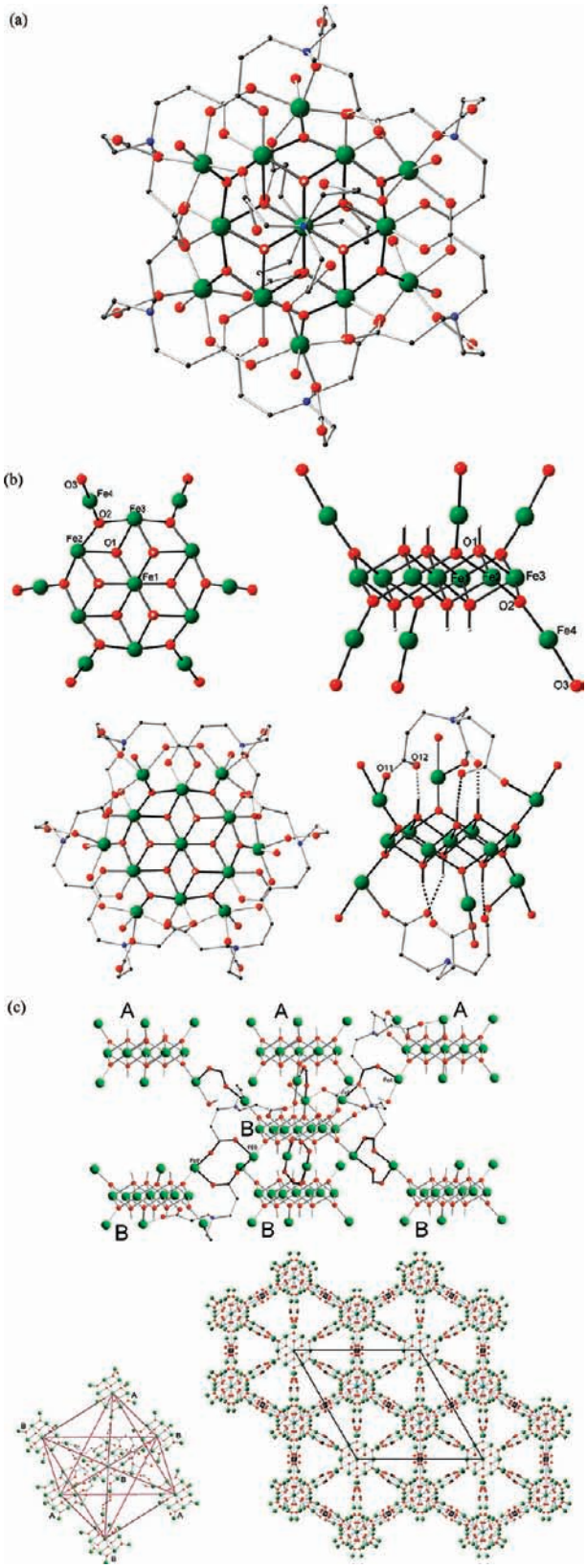

Figure 10. Structural features of Fe_{13}. (a) One complete $[Fe_{13}(\mu_3\text{-}OH)_6(\mu_3\text{-}O)_6(H_2O)_6(Hntp)_8]^{5+}$ cluster. (b) $[Fe_{13}(\mu_3\text{-}OH)_6(\mu_3\text{-}O)_6(H_2O)_6]^{21+}$ core in $[Fe_{13}(\mu_3\text{-}OH)_6(\mu_3\text{-}O)_6(H_2O)_6(Hntp)_8]^{5+}$and the coordination of the $Hntp^{2-}$-ligands to this core. (c) Connections between the A- and B-type clusters. Linkage of a B-type cluster with its six surrounding neighbors showing the octahedral arrangement of the clusters and the 3D packing arrangement of the compound viewed down the *c* axis; most of the ligand atoms have been omitted for clarity. Color code: green, Fe; red, O; blue, N; black, C; white, H.

structures. In **7** and **8**, the central iron(II) and sodium ions are, respectively, linked to six iron(III) ions on the rim by six μ_3-alkoxo bridges. Each iron(III) ion on the rim has an N_1O_5 chromophore with coordination bond lengths of Fe−O = 1.877(3)−2.078(3) Å and Fe−N = 2.074(4) Å for **7** and Fe−O = 1.903(3)−2.122(3) Å and Fe−N = 2.112(3) Å for **8**, while the central iron(III) and sodium ions are coordinated by oxygen atoms with coordination bond lengths of 2.164(3) and 2.344(2) Å, respectively.

$[Fe^{III}_3(bmsae)_3Cl_2(MeOH)(OMe)]\cdot MeOH\cdot Et_2O$ (**9**) crystallized in the monoclinic space group of $P2_1/n$, and three iron(III) ions comprise an incomplete cubic core by a μ_3-methoxo bridge and three μ_2-alkoxo groups from $bmsae^{2-}$. Two iron(III) ions have NO_4Cl_1 coordination, while the other one has N_1O_5 coordination. Coordination bond lengths are Fe−N = 2.107(3)−2.128(3) Å, Fe−O = 1.890(3)−2.107(3) Å, and Fe−Cl = 2.229(1)−2.322(1) Å.

$[Fe^{III}_2(Hbmsae)_2(OMe)_2Cl_2][Fe_3(bmsae)_3(OMe)Cl_2(MeOH)]_2\cdot 1.5MeOH$ (**10**) crystallized in the monoclinic space group $P2_1$. **10** is composed of one dinuclear and two trinuclear complex molecules in the crystal. The trinuclear unit has a structure similar to that of **9**, and two iron(III) ions in the dinuclear units have $N_1O_4Cl_1$ coordination and are doubly bridged by μ_3-methoxides. Coordination bond lengths for the dinuclear unit are Fe−N = 2.146(10)−2.083(9) Å, Fe−O = 1.927(7)−2.054(7) Å, Fe−Cl = 2.302(3)−2.319(3) Å.

Mössbauer Spectra. ^{57}Fe Mössbauer spectra of **6**−**10** were measured at 20 K (Figure 12), and Mössbauer parameters (relative to iron steel) are listed in Table 3. **6** showed two quadrupole doublets with a peak ratio of 0.85:0.15. Mössbauer parameters of isomer shift (δ) and quadrupole splitting (ΔE_Q) are δ = 1.19 mm s^{-1} with ΔE_Q = 1.46 mm s^{-1} and δ = 1.19 mm s^{-1} with ΔE_Q = 1.46 mm s^{-1}, suggesting that all iron ions are HS Fe^{2+} species. The Mössbauer spectrum of **7** exhibits two quadrupole doublets, of which the parameter sets [(δ = 1.18 mm s^{-1} and ΔE_Q = 1.47 mm s^{-1}) and (δ = 0.50 mm s^{-1} and ΔE_Q = 0.42 mm s^{-1})] are characteristic of HS Fe^{2+} and HS Fe^{3+} ions, respectively. Assuming that the Mössbauer−Lamb factors for the Fe^{3+} and Fe^{2+} ions have similar values, the Fe^{3+}/Fe^{2+} ratio calculated from the peak areas is 0.18:0.82, which is in good agreement with the ratio of 1:6 (=0.14:0.86) determined for the chemical formula. Mössbauer spectra of **8**−**10** consist of one, two, and three quadrupole doublets, respectively, and the Mössbauer parameters suggest that all iron atoms are HS Fe^{3+} ions.

Magnetic Properties. Magnetic susceptibility measurements for **6**−**10** were performed in the temperature range of 1.8−300 K, and the χ_mT−T plots are shown in Figure 13.

The χ_mT value of **6** is 23.7 emu mol^{-1} K at 300 K, which is slightly larger than the value (21.0 emu mol^{-1} K) expected for the uncorrelated seven HS Fe^{2+} ions (g = 2.0 and S = 2). The χ_mT values gradually increased as the temperature was lowered, reaching the maximum value of 59.7 emu mol^{-1} K at 5.5 K. Magnetic susceptibility data suggest that **6** has a substantial HS ground state; however, the maximum χ_mT value is considerably smaller than the one (105 emu

Scheme 3. Synthetic Routes

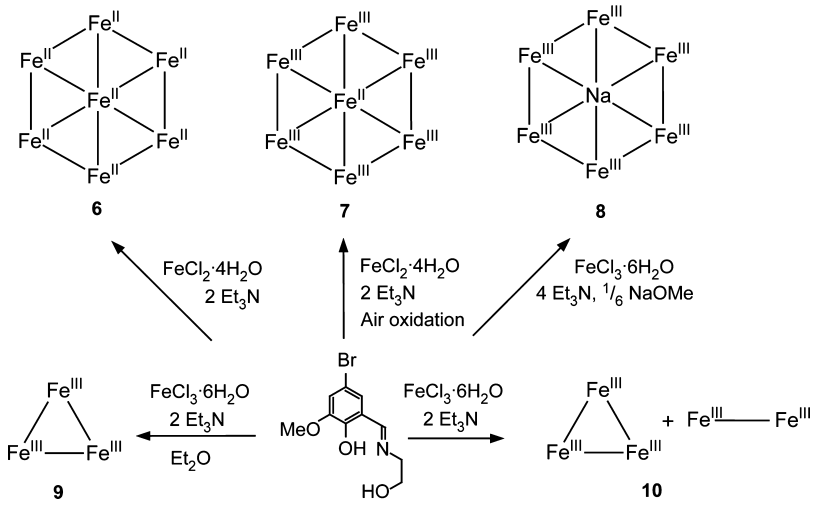

mol^{-1} K) for an $S = 14$ state resulting from the parallel spin alignments of the seven Fe^{2+} ions in the wheel. The spin Hamiltonian of $H = -2J_1\hat{S}_0\cdot(\hat{S}_1 + \hat{S}_2 + \hat{S}_3 + \hat{S}_4 + \hat{S}_5 + \hat{S}_6) - 2J_2(\hat{S}_1\cdot\hat{S}_2 + \hat{S}_2\cdot\hat{S}_3 + \hat{S}_3\cdot\hat{S}_4 + \hat{S}_5\cdot\hat{S}_6 + \hat{S}_6\cdot\hat{S}_1)$, where J_1

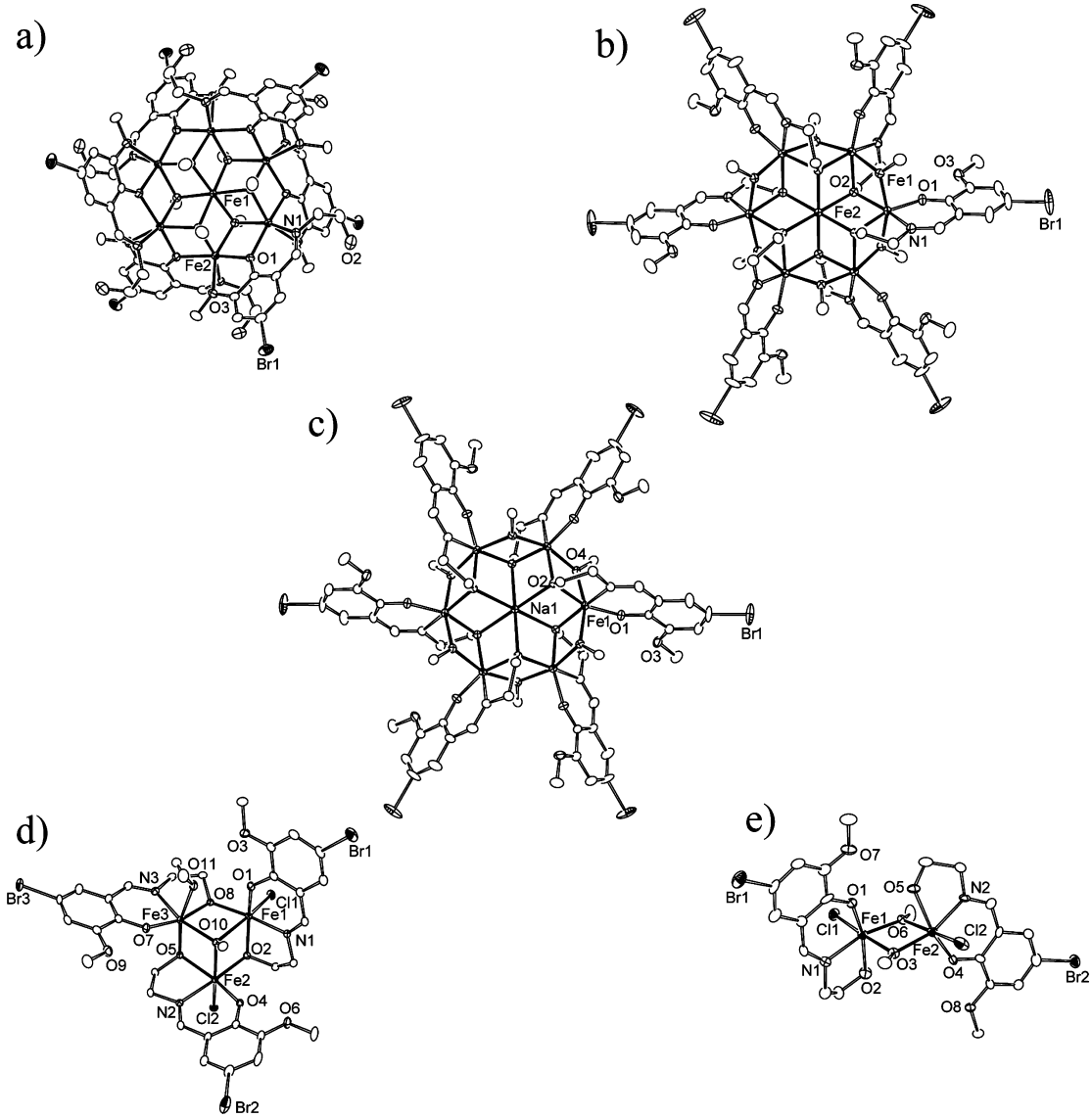

Figure 11. ORTEP diagrams of complex molecules: (a) $[Fe^{II}_7(Hbmsae)_6(OMe)_6]Cl_2$ (**6**), (b) $[Fe^{II}Fe^{III}_7(bmsae)_6(OMe)_6]Cl_2$ (**7**), (c) $[NaFe^{III}_6(bmsae)_6(OMe)_6]Cl$ (**8**), (d) $[Fe^{III}_3(bmsae)_3Cl_2(OMe)(MeOH)]$ (**9**), and the dinuclear unit of $[Fe^{III}_2(Hbmsae)_2(OMe)_2Cl_2][Fe_3(bmsae)_3(OMe)Cl_2(MeOH)]_2$ (**10**).

Table 2. Crystallographic Data for **6**−**10**

	6	**7**	**8**	**9**	**10**
formula	$C_{66}H_{96}Br_6\ Cl_2Fe_7N_6O_{30}$	$C_{66}H_{124}Br_6\ Cl_2Fe_7N_6O_{47}$	$C_{66}H_{138}Br_6Cl\ Fe_6N_6NaO_{54}$	$C_{37}H_{51}Br_3\ Cl_2Fe_3N_3O_{13}$	$C_{88.5}H_{112}Br_8\ Cl_6Fe_8N_8O_{32.5}$
fw	2394.80	2695.02	2752.82	1223.99	3106.64
space group	$R\bar{3}$	$Ia\bar{3}d$	$Ia\bar{3}d$	$P2_1/n$	$P2_1$
a/Å	14.8631(7)	37.3339(18)	37.1998(5)	11.6626(5)	11.6949(7)
b/Å				18.7616(9)	14.2529(9)
c/Å	36.460(3)			21.613(1)	34.705(2)
β/deg				96.154(1)	90.072(1)
V/Å^3	6975.4(7)	52037(4)	51478(1)	4702.0(4)	5784.8(6)
Z	3	16	16	4	2
T/°C	−73	−73	−143	−73	−73
ρ_{calcd}/g cm^{-3}	1.710	1.376	1.421	1.729	1.784
μ/mm^{-1}	3.772	2.714	2.625	3.638	3.951
$R1^a$	0.0663	0.0720	0.0690	0.0501	0.0521
$wR2^b$	0.2075	0.2070	0.1825	0.1203	0.1148

^{a} $R1 = \sum||F_o| - |F_c||/\sum|F_o|$. ^{b} $wR2 = \{\sum[w(F_o^2 - F_c^2)^2]/\sum[w(F_o^2)^2]\}^{0.5}$.

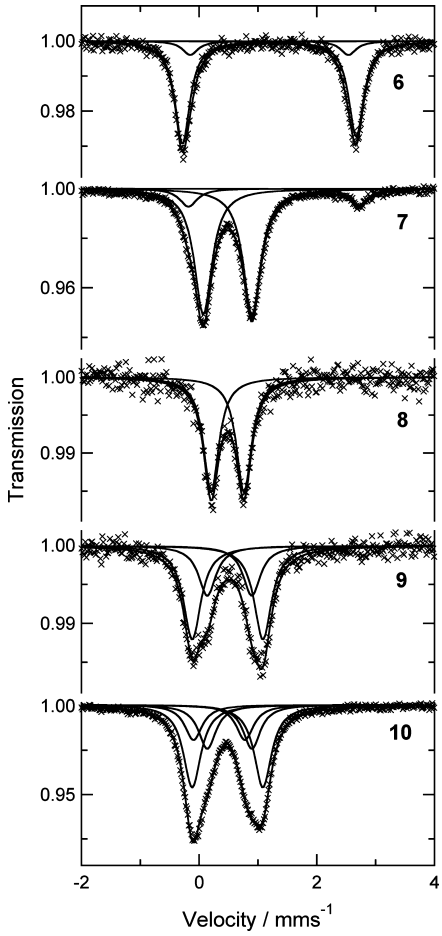

Figure 12. ^{57}Fe Mössbauer spectra of **6**−**10** measured at 20 K.

and J_2 represent exchange coupling constants between the $Fe^{2+}{}_{rim}$−$Fe^{2+}{}_{center}$ and $Fe^{2+}{}_{rim}$−$Fe^{2+}{}_{rim}$, respectively, was used to analyze the magnetic data of **6**. A modified vector-coupling model was applied to estimate exchange-coupling constants,[43] where the powder magnetic susceptibility data in the temperature range of 20−300 K were used and the contribution from the magnetic anisotropy and intermolecular magnetic interactions was neglected. The interaction paths were taken into account by use of the Kambe-type vector-coupling scheme, and the redundant paths were compensated for by using the first-order perturbation terms. Least-squares fits converged on the parameters of $g = 2.08(1)$, $J_1 = 3.32(2)$ cm^{-1}, and $J_2 = -1.12(1)$ cm^{-1} under the conditions of $J_1 > 0$ and $J_2 < 0$. The parameters suggests that the ground spin state is $S = 10$ and the first and second excited states of $S = 11$ and 9 are 0.66 and 0.88 cm^{-1} higher than the ground state, respectively. The population on each spin state at 1.8 K is 44% for the ground state $S = 10$, 26% for $S = 11$, and 22% for $S = 9$. Note that the analysis of magnetization data at 1.8 K yielded a D value of −0.17 cm^{-1}, supposing the $S = 10$ spin ground state. Alternating current (ac) magnetic susceptibility of **6** was measured for a polycrystalline sample in the temperature range of 1.8−3.6 K with a 3 G ac field oscillating at 25−6000 Hz. Both in-phase and out-of-phase signals are frequency-dependent (Figure 14). Although χ_m'' versus T plots did not show peak maxima in the temperature range measured, the data might suggest that **6** is a class of SMM.

Magnetic susceptibility measurements for **7**−**10** revealed that intramolecular antiferromagnetic interactions are operative among iron centers. The $\chi_m T$ values for **7**−**10** are 19.4, 17.5, 8.3, and 23.9 emu mol^{-1} K at 300 K, respectively, which are considerably smaller than the values expected for the sums of the Curie constants (29.3, 26.3, 13.1, and 35.0 emu mol^{-1} K with $g = 2.0$) of component Fe^{3+} ions.

The complex molecule of **7** has the same core structures as **6**, and the same spin Hamiltonian and exchange-coupling constants as those of **6** were used to analyze the magnetic data for **7**. Spins in **7** are frustrated because of the intramolecular antiferromagnetic interactions, suggesting the several spin states jostling in the lower energy region. The analysis of the magnetic data was not, therefore, straightforward, and least-squares fits were not properly converged. The relative error surface was generated as a function of J_1 and J_2 with the fixed g value of 2.0, where the root-mean-square (rms) error σ for the data points of n was calculated using eq 1. The 3D surface plot of the rms errors showed no minimum (Figure 15a).

$$\sigma = \left[\frac{\sum(\chi_{calcd} - \chi_{exptl})^2}{n}\right]^{1/2} \quad (1)$$

8 has the wheel structure with a diamagnetic sodium at the center; the molecule can, therefore, be treated as a six-membered antiferromagnetic ring with an $S = 0$ spin ground

(43) Asano, K.; Inoue, K.; Nakano, M.; Miyazaki, Y.; Sorai, M.; Nakatani, K.; Kahn, O. *Bull. Chem. Soc. Jpn.* **1999**, *72*, 1749.

Table 3. Mössbauer Parameters for **6**−**10**[a]

6			7			8		9			10		
δ	ΔE_Q	R	δ	ΔE_Q	R	δ	ΔE_Q	δ	ΔE_Q	R	δ	ΔE_Q	R
1.19	2.95	0.88	1.27	2.90	0.12	0.48	0.56	0.48	1.20	0.65	0.48	1.20	0.51
1.19	2.69	0.12	0.48	0.83	0.88			0.52	0.76	0.35	0.52	0.76	0.27
											0.34	0.87	0.22

[a] The parameters δ (mm s^{-1}) are relative to iron steel, and the R values are relative to peak ratios.

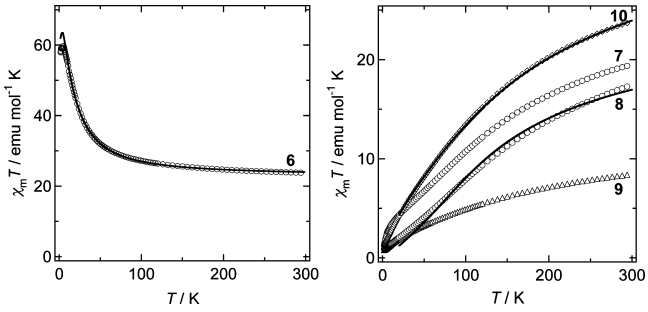

Figure 13. $\chi_m T$ versus T plots for **6**−**10**. Solid lines are reproduced by least-squares fits using the parameters described in the text.

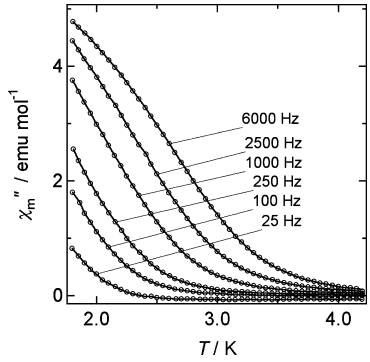

Figure 14. χ_m'' versus T plots of **6**.

state. The spin Hamiltonian employed is $H = J(-\hat{S}_{ring}^2 + \hat{S}_{even}^2 + \hat{S}_{odd}^2) + 2J\,(\hat{S}_1 \cdot \hat{S}_4 + \hat{S}_2 \cdot \hat{S}_5 + \hat{S}_3 \cdot \hat{S}_6)$, where $\hat{S}_{odd} = \hat{S}_1 + \hat{S}_3 + \hat{S}_5$, $\hat{S}_{even} = \hat{S}_2 + \hat{S}_4 + \hat{S}_6$, and $\hat{S}_{ring} = \hat{S}_{odd} + \hat{S}_{even}$. J represents the exchange-coupling constant between iron(III) centers. The expression of χ_m was derived by using a Kambe's model with a perturbative correction, and the J value of -7.13 cm^{-1} was obtained with $g_{Fe} = 1.99$.

9 consists of an isosceles triangle core doubly bridged by an alkoxo group, and the intramolecular antiferromagnetic interactions are operative in the core. The spin Hamiltonian of $H = -2J_1\hat{S}_1 \cdot \hat{S}_2 - 2J_2(\hat{S}_1 \cdot \hat{S}_3 + \hat{S}_2 \cdot \hat{S}_3)$ was employed in the analysis of the magnetic data; however, the least-squares fit was diverged. The rms error surface plot did not show a single minimum σ value, which is due to the spin frustration in the core (Figure 5b).

10 contains one dinuclear and two trinuclear units in the crystal, and the latter has a structure similar to that of **9**. In the analyses of magnetic data of **10**, the contribution of the trinuclear units was subtracted from the total susceptibility data of **10**, and the exchange-coupling constant of $J = -9.12$ cm^{-1} with $g = 2.0$ was obtained for the dinuclear unit.

Conclusions and Outlook. In this paper, we have shown how compounds possessing structural motifs derived from an $\{Fe_7(\mu_3\text{-}OR)_6(\mu\text{-}OR)_6\}$ core can show a variety of interesting magnetic properties. Some of these can be difficult to unravel often as a result of the system containing HS Fe^{III} ions that lead to the presence of many possible pairwise interactions. However, the survey of compounds already in the literature shows that such systems can have high ground spin states and act as SMMs. Furthermore, ligand shells encapsulating the core motifs can be derivatized, leading to changes in the system, both within the core and throughout the crystal as a result of packing preferences. In such ways, a certain amount of control over the properties of the compounds can be exerted.

In syntheses of new metal complexes, we sometime obtain mixtures of products in a mushy slurry. In the reaction of Schiff base ligands with iron sources, crystals with different morphologies were growing in the beaker. The X-ray structure determination of each crystal, which was carefully picked out by hand, allowed us to know what we had in the reaction mixture. We isolated each species by changing the reaction conditions. Although this process requires both experience and patience, we are able to embark on the study of a new series of magnetically interesting clusters. Overall, iron-based systems would appear to offer many possibilities in the development of molecular-based magnets.

Experimental Section

Synthetic Procedures. All reagents were obtained from commercial suppliers and were used without further purification. Schiff base ligand H_2bmsae was prepared by the condensation reactions of 5-bromo-3-methoxysalicylaldehyde with 2-aminoethanol. **6** was prepared under a nitrogen atmosphere with Schlenk techniques, and the other complexes were prepared in air.

$[Fe^{II}_7(Hbmsae)_6(OMe)_6]Cl_2 \cdot 6H_2O$ (6). H_2bmsae (274 mg, 1.0 mmol) was dissolved in methanol (20 mL), and triethylamine (202 mg, 2.0 mmol) was added. To the resultant solution was added $FeCl_2 \cdot 4H_2O$ (233 mg, 1.17 mmol) in 10 mL of methanol. After standing for several days, dark-red hexagonal plates were obtained. Anal. Calcd for $C_{66}H_{96}Br_6Cl_2Fe_7N_6O_{30}$: C, 33.10; H, 4.04; N, 3.51. Found: C, 32.90; H, 3.98; N, 3.20.

$[Fe^{II}Fe^{III}_6(bmsae)_6(\mu_3\text{-}OMe)_6]Cl_2 \cdot 23H_2O$ (7). H_2bmsae (137 mg, 0.5 mmol) was dissolved in methanol (20 mL), and triethylamine (101 mg, 1.0 mmol) was added. To the resultant solution was added $FeCl_2 \cdot 4H_2O$ (233 mg, 1.17 mmol) in 10 mL of methanol. After standing for several days, black hexagonal plates were obtained. Anal. Calcd for $C_{66}H_{102}Br_6Cl_2Fe_7N_6O_{36}$: C, 27.57; H, 5.05; N, 2.92. Found: C, 27.17; H, 4.83; N, 2.73.

$[NaFe^{III}_6(bmsae)_6(\mu_3\text{-}OMe)_6]Cl \cdot 30H_2O$ (8). H_2bmsae (27 mg, 0.10 mmol) was dissolved in methanol (30 mL), and triethylamine (40 mg, 0.40 mmol) and 28% sodium methoxide/methanol solution (3.2 mg, 0.017 mmol) were added. To the resultant solution was added anhydrous $FeCl_3$ (16 mg, 0.10 mmol) in 10 mL of methanol. After standing for several days, black hexagonal plates were obtained. Anal. Calcd for $C_{66}H_{102}Br_6ClFe_6N_6NaO_{36}$: C, 32.64; H, 4.23; N, 3.46. Found: C, 32.85; H, 4.17; N, 3.24.

$[Fe^{III}_3(bmsae)_3Cl_2(MeOH)(OMe)] \cdot MeOH \cdot Et_2O$ (9). H_2bmsae (273 mg, 1.0 mmol) was dissolved in methanol (20 mL), and a

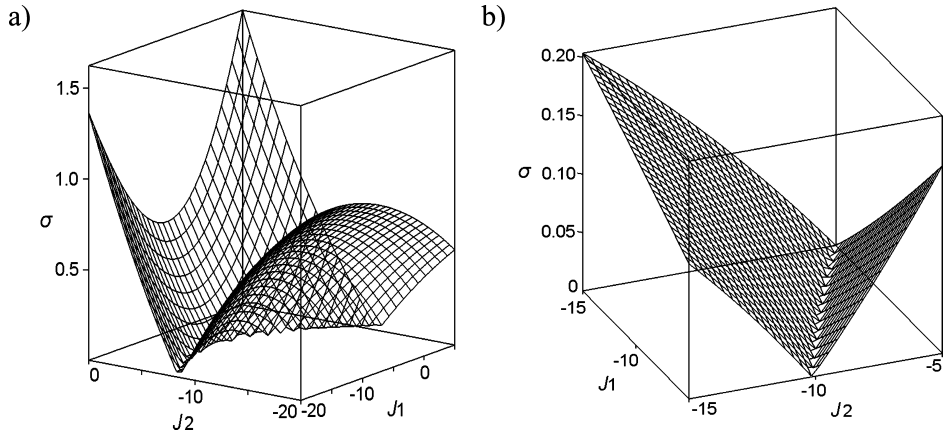

Figure 15. 3D plots of the rms error surface for (a) **7** and (b) **9**.

28% sodium methoxide/methanol solution (386 mg, 2.0 mmol as NaOMe) was added. To the resultant solution was added anhydrous $FeCl_3$ (160 mg, 1.0 mmol) in 10 mL of methanol. Black plate-like crystals were obtained by slow diffusion of Et_2O vapor in a sealed tube. Anal. Calcd for $C_{33}H_{41}Br_3Cl_2Fe_3N_3O_{12}$: C, 34.47; H, 3.59; N, 3.65. Found: C, 34.51; H, 3.53; N, 3.48.

$[Fe^{III}_2(Hbmsae)_2(OMe)_2Cl_2][Fe_3(bmsae)_3(OMe)Cl_2(MeOH)]_2 \cdot 1.5MeOH$ (10). H_2bmsae (273 mg, 1.0 mmol) was dissolved in methanol (5 mL), and triethylamine (202 mg, 2.0 mmol) was added. To the resultant solution was added anhydrous $FeCl_3$ (160 mg, 1.0 mmol) in 5 mL of methanol. After standing for 6 h, a dark-blue microcrystalline solid was precipitated and collected by suction. Microcrystallites were placed in the mother solution, and black hexagonal plates were obtained after several days. Anal. Calcd for $C_{86}H_{102}Br_8Cl_6Fe_8N_8O_{30}$: C, 34.13; H, 3.40; N, 3.70. Found: C, 32.47; H, 3.00; N, 3.60.

Physical Measurement. Magnetic susceptibility data were collected in the temperature range of 1.8−300 K and in an applied field of 500 G of a Quantum Design model MPMS-XL SQUID magnetometer. Pascal's constants were used to determine the diamagnetic corrections.

X-ray Data Collection and Structure Refinements. Crystal data collection and refinement parameters for **6**−**10** are given in Table 2. Suitable crystals for X-ray data collection were selected and mounted with an epoxy resin on the tip of a glass fiber. Diffraction data were collected at −73 °C on a Bruker SMART APEX diffractometer fitted with a CCD-type area detector using monochromated Mo Kα radiation (λ = 0.710 73 Å). The data frames were integrated using *SAINT* (Bruker Analytical X-ray Systems), and empirical absorption corrections were applied by *SADABS* (G. M. Sheldrick, 1994). The structures were solved by direct methods and refined by the full-matrix least-squares method on all F^2 data using the *SHELXTL* program package (Bruker Analytical X-ray Systems). Non-hydrogen atoms were refined with anisotropic thermal parameters. Hydrogen atoms were included in calculated positions and refined with isotropic thermal parameters riding on those of the parent atoms.

Supporting Information Available: X-ray crystallographic data in CIF format of **6**−**10**. This material is available free of charge via the Internet at http://pubs.acs.org.

IC801776W